Available online at www.sciencedirect.com
ScienceDirect
Journal of Applied Geophysics 63 (2007) 68–79
JOURNAL OF APPLIED GEOPHYSICS
www.elsevier.com/locate/jappgeo

# Shallow velocity–depth model using first arrival traveltime inversion at the $CO_2$SINK site, Ketzin, Germany

Sawasdee Yordkayhun [a,*], Christopher Juhlin [a], Ruediger Giese [b], Calin Cosma [c]

[a] *Department of Earth Sciences, Uppsala University, Villavägen 16, SE-75236 Uppsala, Sweden*
[b] *GeoForschungsZentrum, Section 5.1, Potsdam, Germany*
[c] *Vibrometric Oy, Vantaa, Finland*

Received 15 February 2007; accepted 24 May 2007

**Abstract**

The $CO_2$SINK project, a carbon dioxide storage and monitoring project, has been in operation in the Ketzin area, Germany since 2004. Goals are to investigate the techniques and understand the processes related to geological storage of $CO_2$ in a saline aquifer. A key element of the project is comprehensive monitoring and the development of verification methods to track the long term spread of the injected $CO_2$. Time lapse seismic surveys in 3D and 2D are important monitoring components for tracking the movement of $CO_2$. Prior to the 3D baseline seismic survey in 2005, a pilot seismic survey was performed in 2004 in order to provide input parameters for the 3D survey and information on target depth. This pilot study, consisting of two perpendicular 2.4 km long profiles confirmed the geological structure based on 1960s vintage seismic data. However, the image is rather poor in the uppermost parts of the seismic sections. In order to obtain additional structural information and to improve the velocity function estimates, first arrival traveltimes were used to image the near-surface structure and to provide an improved velocity function for interpretation of reflection data. We used a generalized linear inversion (GLI) method, based on iterative least-squares inversion, to reconstruct the velocity–depth model. A simple and smooth starting velocity model was derived from traveltime plots and the stacked reflection seismic sections. Reliability of the resulting velocity models were estimated from analysis of the traveltime residuals (RMS error) and qualitative analysis of ray coverage. There appears to be a good correlation of layer boundaries in our model and higher amplitude reflections observed on the stacked sections. Comparison of the seismic depth sections computed using stacking velocities with the GLI inverted velocity shows that the depth sections obtained from the latter agrees better with the velocity models. The combination of borehole data and the depth converted stacked sections provides key constraints for interpretation of the velocity models. The estimated investigation depth of the seismic profiles is on the order of 400 m with rays penetrating the surface cover and sedimentary sequences. These sedimentary rocks are characterized by a gradual increase in the velocity field with depth without strong contrasts and insignificant lateral velocity variations.


*Keywords:* Traveltime inversion; Generalized linear inversion; Velocity–depth model; $CO_2$SINK project

## 1. Introduction

Carbon dioxide ($CO_2$) sequestration is an option and opportunity for reducing $CO_2$ emissions into the atmosphere by capturing $CO_2$ and injecting it into

* Corresponding author. Tel.: +46 18 471 7161; fax: +46 18 501110.
*E-mail address:* sawasdee.yordkayun@geo.uu.se (S. Yordkayhun)

0926-9851/$ - see front matter © 2007 Elsevier B.V. All rights reserved.
doi:10.1016/j.jappgeo.2007.05.001

deep geological formations (Arts et al., 2004; White et al., 2004; IPCC, 2005). The EU funded $CO_2$SINK project is an integrated project focusing on small scale geological storage and monitoring of $CO_2$ (Förster et al., 2006) and was initiated in 2004. Its main objectives are to (1) investigate and advance the understanding of the science and practical processes related to geological storage of $CO_2$ in a saline aquifer, (2) build confidence towards future European geological storage of $CO_2$, and (3) provide real case experience that can be used in the development of future regulatory frameworks for geological storage of $CO_2$. The test site is located west of Berlin, near the town of Ketzin, Germany (Fig. 1). It lies close to a suitable anticlinal structure and the infrastructure from a natural gas storage facility, that was abandoned in 2004, is still partially in place. Plans are to drill three boreholes, one injection borehole and two observation boreholes with a spacing of about 50–100 m, into the flank of the Ketzin anticline. Nearly pure $CO_2$ will be injected at about 650 m depth into a saline sandstone aquifer at the rate of approximately 100 tons/day for a period of up to 2 years. An important component of the project is the monitoring of the $CO_2$ movement using seismic methods. Seismic monitoring methods that will be applied include cross-well, vertical seismic profile (VSP), moving source profiling (MSP), 2D and 3D time lapse techniques. As part of this program, a 3D seismic baseline survey was acquired in

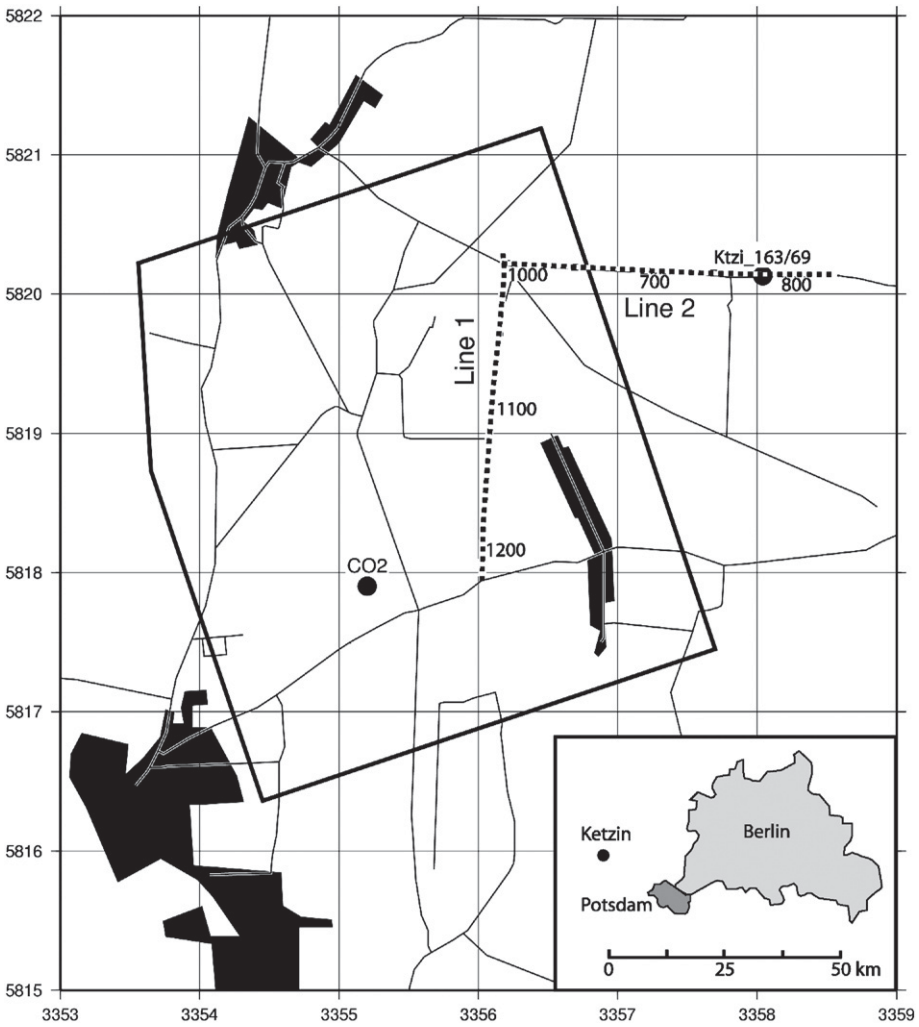


Fig. 1. Map of the Ketzin pilot study area west of Berlin, Germany. The two CDP profiles are marked as Line 1 (N–S profile) and Line 2 (E–W profile). Borehole Ktzi 163/69 is indicated by the black circle. The area marked by the polygon approximately encloses the area for the main 3D survey. The expected injection site ($CO_2$) is also indicated.

2005 (Juhlin et al., 2007). Prior to this 3D survey a pilot study (Yordkayhun et al., submitted for publication), consisting of two 2.4 km long perpendicular profiles, was carried out to test various field parameters and acquisition strategies. It is the data from these two profiles, in particular data relating to the near-surface, that are used as input to the study presented in this paper.

Near-surface seismic imaging techniques have been widely demonstrated and used in an increasing number of applications (Steeples and Miller, 1990; Buker et al., 1998; Juhlin et al., 2002). One of the difficult issues in reflection seismic processing is that poor images are generally obtained in the upper part of the sections due to shot-associated noise, surface waves, and direct arrivals that obscure the reflected energy (Miller et al., 1998). In many cases, the shallowest reflections must be removed prior to normal moveout (NMO) corrections and stacking, resulting in that details from the upper part of the section are generally lost. In addition, heterogeneities in the near-surface lead to static correction problems. Therefore, joint interpretation of refraction and reflection seismic data from the near-surface can have many benefits. Numerous sophisticated interpretation techniques of refraction seismic data and tomographic inversion schemes on how to better image the near-surface have been extensively discussed in the geophysical literature (e.g., Hampson and Russell, 1984; Lines and Treitel, 1984; Marsden, 1993; Macrides and Dennis, 1994; Belfer and Landa, 1996; Lanz et al., 1998; Taner et al., 1998; Marti et al., 2002; Bergman et al., 2004). In this study, traveltime inversion techniques based on the generalized linear inversion (GLI) method proposed by Hampson and Russell (1984) have been used. The aims of this study were to obtain information on near-surface structures (e.g., shallow aquifers, thickness of the cover) which are important for long term monitoring and to improve the time to depth conversion of the seismic reflection sections. Once the shallow velocity–depth models were constructed using the first arrival refraction traveltime data from the pilot study, the models were compared to stacked sections and borehole data in order to obtain near-surface information and aid in interpretation of the seismic reflection sections.

## 2. Previous work

Prior to carrying out the 3D baseline seismic survey (Juhlin et al., 2007), a pilot study was performed in 2004 (Yordkayhun et al., submitted for publication). The main goals of the pilot study were to (1) evaluate the response of the Ketzin site to reflection seismics, especially at the planned injection depth, (2) test different acquisition parameters, such as surface seismic sources, geophone types and deployment, and recording parameters, and (3) use the results to guide the planning of the 3D survey. Two perpendicular seismic profiles were acquired along two agricultural roads near the target area of the planned 3D survey (Fig. 1). The N–S profile (Line 1) was a traditional agricultural road, while the E–W profile (Line 2) consisted of hard soil that had been compressed by heavy military equipment. Data were recorded by a 240 channel (fixed spread) SERCEL 408 system. All 120 geophones per line were laid out at an interval of 20 m. Three different sources, MiniVib, weight drop, and VIBSIST (Park et al., 1996; Cosma and Enescu, 2001) were activated along the two lines using the same recording scheme. Analysis of shot gathers and CDP stacked sections from the three sources form the basis for a paper covering the comparison of the sources (Yordkayhun et al., submitted for publication). In this study we use the stacked sections from the VIBSIST source as a starting point for first arrival traveltime inversion and as an aid interpreting the resulting velocity models.

## 3. Data

Picked first arrival traveltimes from the reflection seismic data were used as input in this study. Shots recorded by the weight drop source were used since the timing of this source was considered to be the most accurate compared to the data recorded by the VIBSIST and MiniVib sources. On raw shot records, data quality is mainly degraded by ground roll, wind and cultural noise from traffic on the roads (Fig. 2). Topography and surface conditions along the profiles may also degrade the data quality in spite of the topography being relatively flat. The surface relief along Line 1 is greater than that of Line 2, suggesting that static shifts may influence the stacked sections more on this line. Picking of first breaks was done using an automatic picking routine and were later edited manually. Great care was taken in the picking, since time shifts due to traveltime errors lead to non-reliable models of the sub-surface (Bais et al., 2003). In the automatic picking routine, the first break times were controlled by a guide function and a narrow band search window (uncertainty of 20 ms), to constrain the picked time at the first positive peak (reverse polarity display). Using the positive peak is suitable for low signal-to-noise ratio data. Almost all of the automatic picks were good in the first pass of picking with most of the mis-picks appearing at the near and far offsets. The picking errors encountered at near offset were due to signal interference from ground roll and at far offsets from ambient noise. To avoid picking the incorrect phase, some portions of the far offsets were not picked on some shot records (Fig. 2).

## 4. Methodology

First arrivals represent refracted energy that has propagated along the fastest path in the sub-surface before arriving at the surface. Processing and interpretation techniques that involve analysis of these traveltimes are well known and a number of popular methods are in use. Recent advances in inversion of seismic refraction data have made it possible to image heterogeneous media, as well as solving static correction problems (e.g., Olsen, 1989; Boschetti et al., 1996; Bergman et al., 2004). Here, we used the first arrival inversion technique proposed by Hampson and Russell (1984), the generalized linear inversion (GLI) method. It is based on ray-tracing through a best-guess initial velocity model and solving the problem of optimizing the fit of the calculated to observed traveltimes in a least-squares sense (Lines and Treitel, 1984; Menke, 1984). The model update procedure for either depth or velocity consists of a looping process that is similar to that used in tomographic inversion. The method is briefly outlined:

(1) An initial velocity model is setup using a decimated set of picked traveltimes for velocity control points. Approximate velocities, layer thicknesses and number of layers are constrained by these traveltime curves.
(2) Theoretical first arrival traveltimes are calculated by the ray-tracing method from each shot–receiver pair.
(3) The traveltime residual (error), the difference between the picked first arrival times and the theoretical first arrival times are calculated. If the actual first break times for each trace are $P_k$, the inverse problem is given by minimizing the objective function (Hampson-Russell Software Services Ltd., 2004):

$$J = \sum_k (P_k - T_k)^2 = \sum_k (P_k - M_k(E, D_i, V_i))^2 \quad (1)$$

where $T_k$ is the predicted first break times for the $k$th trace, $M_k$ is the modeling function, i.e., ray-tracing. $E$, $D_i$ and $V_i$ are model parameters: elevation of the surface, elevation of the base of the $i$th layer and velocity within the $i$th layer, respectively.
(4) Since Eq. (1) is non-linear in the unknown parameters, the GLI algorithm solves the equation by linearizing it in the vicinity of the initial guess and updating the thickness and velocities of the layers. This procedure is repeated until some acceptable correspondence is reached between observed and model first break picks. In practice, this update procedure is calculated by the Gauss–Seidel and conjugate-gradient algorithms.
(5) Eq. (1) is solved based on the optimum geological model or long-wavelength problem, assuming a simple relatively small number of layers and smoothing of layer thicknesses and velocities. The

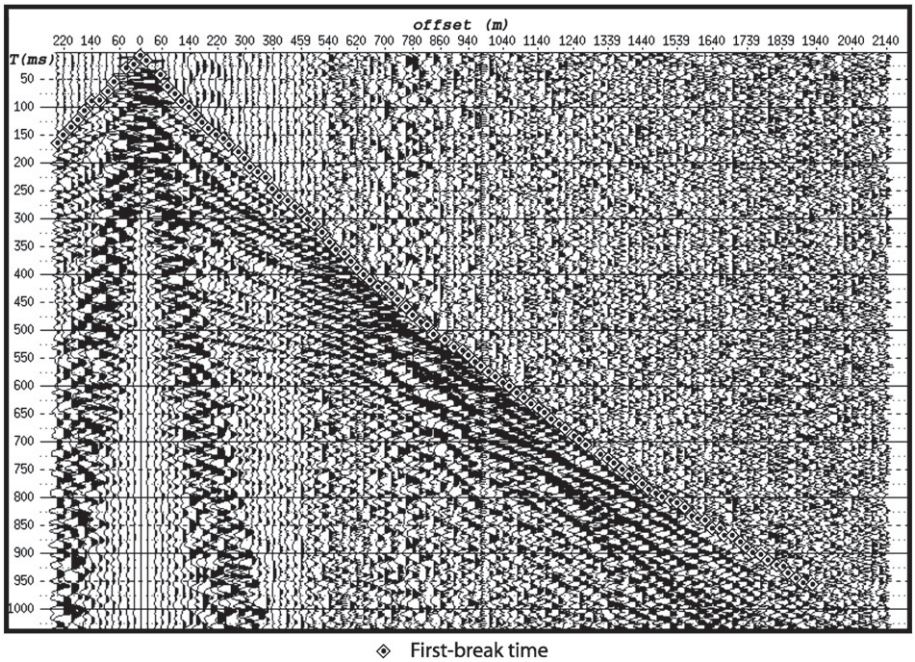


Fig. 2. A shot record from Line 2 with picked first arrival times marked. Note that low S/N ratios occur at large offsets.

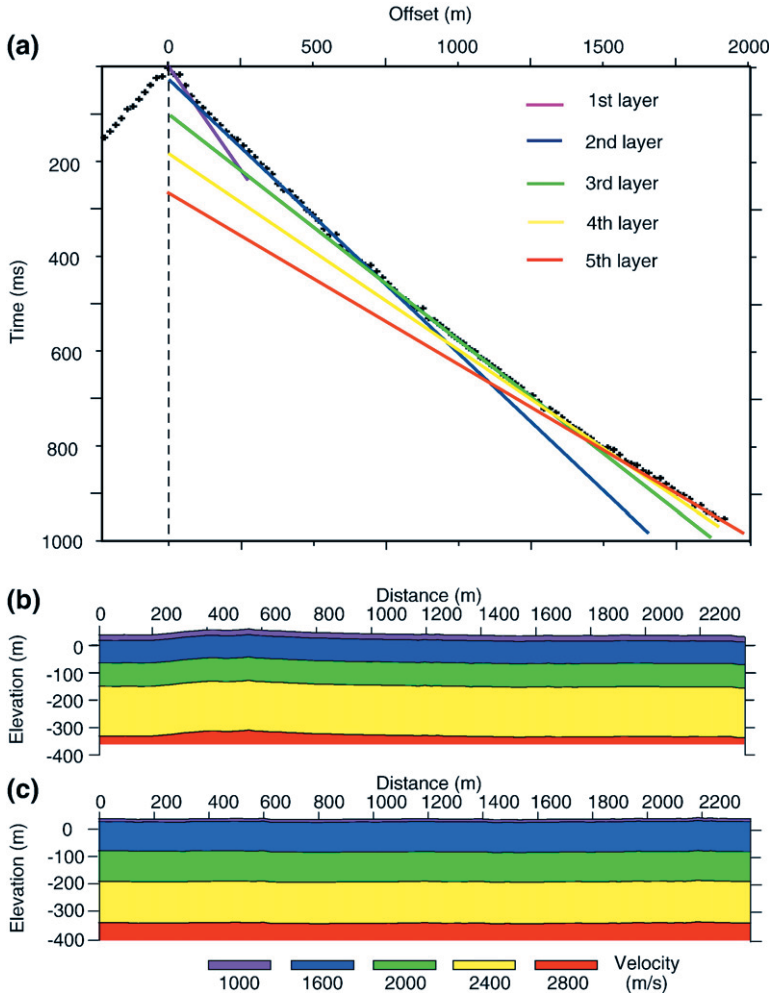


Fig. 3. (a) Initial velocity–depth models as estimated from traveltime curves at each control point based on slope segments and intercept times as a guide. (b) and (c) simple constant velocity and thickness initial models interpolated from (a) of Line 1 and Line 2, respectively.

difference of this model relative to the real complex earth model can be treated as a set of residual surface-consistent time shifts (short-wavelength static or time residuals). In order to recover the high frequency anomalies present in the original first breaks that may be missing from the final model, the short-wavelength time residuals are calculated and applied after the final iteration. By adding the short-wavelength time residual, the predicted first break times can be rewritten as $T_{ks}=T_k+T_R+T_S$. Then the new objective function is:

$$J_s = \sum_k (P_k - T_{ks})^2 = \sum_k (P_k - M_k(E,D_i,V_i) - \xi_k)^2 \quad (2)$$

where $\xi_k=T_S+T_R$=residual error in the $k$th trace, $T_S$ is the short-wavelength time residual for the shot containing trace k and $T_R$ is the short-wavelength time residual for the receiver location of trace $k$.

Once the final velocity–depth models are found, static corrections can be calculated and used in the reflection seismic processing.

## 5. Results

### 5.1. Initial models

In general, non-unique solutions are obtained in real geophysical problems (Scales, 1987). Since a non-linear equation is solved by a linear inversion procedure, we can

Table 1
The main GLI inversion parameters of Line 1 and Line 2

| Inversion parameters | Line 1 | Line 2 |
|---|---|---|
| Geological model iteration | 5 | 5 |
| Conjugate-gradient iteration | 20 | 20 |
| Minimum–maximum offset (m) | 0–2400 | 0–2400 |
| Maximum thickness deviation (m) | 10 | 50 |
| Maximum interval velocity deviation (m/s) | 50 | 100 |
| Threshold for deleting picks | 2 | 2 |
| Short wave statics iterations | 10 | 10 |

never be sure that the solution obtained is the absolute minimum of the objective function. For this reason, the initial guess can have a critical influence on the final answer. In this study, the inversion method was tested by using different initial uniform layered models in order to investigate the influence of the initial guess. Four layer and five layer cases with constant layer thickness, but increasing velocity with depth, were tested as initial models. The inversion method assumes that the velocity of the shallowest layer is known. Analysis of near offset first breaks showed that a velocity of 1000 m/s is representative for the uppermost unconsolidated layer and was chosen as the uppermost velocity in all models. Although the algorithm allows us to vary both the velocity and thickness of the layers at each station, simple initial models consisting of horizontal constant velocity layers matched well the time distance curves from the control points and corresponded roughly to the stacked sections. Both tomographic inversion (not reported on in this paper) and GLI methods were applied to the various initial models. In both cases, lateral velocity variations were small, but RMS errors using tomographic inversion were higher than from the GLI method. Therefore, we focused our studies on the GLI method and assumed that the lateral velocity gradient below the profiles was not significant. After several tests, it was decided to use five layers for the initial model, since the resulting inversions showed more reasonable structures than when using a four layer initial model. See Fig. 3 for the initial models used in this study.

### 5.2. Final models

Similar initial models were used for both profiles, except for the thickness of the layers. After each iteration, the rays traced through the models and the corresponding traveltime residuals were recomputed. Final models were obtained after 5 iterations. Testing the different initial models by varying the layer thickness and velocity resulted in small differences in the final models, except on Line 1 where the near-surface structure is complex. If the same inversion parameters were used in both profiles, stable results were not obtained. However, if the allowed deviation in velocity and layer thickness was reduced on Line 1 (Table 1) then the solution became stable. These conditions imply that a slowly varying model constraint (smoothing constraint) has been imposed on Line 1. Forcing the model to be smooth on Line 1 implies that only the long-wavelength components (calculated from the geological model) are accounted for with the iterative modeling technique. Therefore the short-wavelength components can only be estimated at the end of the iteration process as simple surface-consistent time delays in the final residual. In contrast, on Line 2, only small differences were found in the final RMS errors when the inversion is run with and without the smoothing constraints. The small short-wavelength component on Line 2 is interpreted as due to the flat surface topography in this profile.

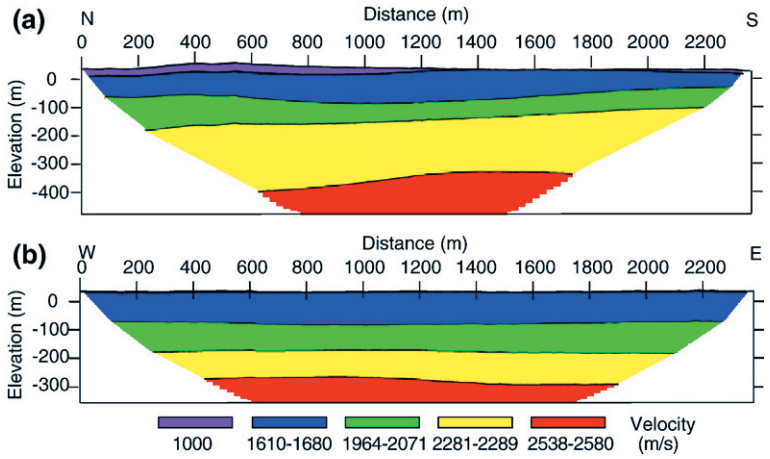


Fig. 4. (a) Velocity–depth model of Line 1. (b) Velocity–depth model of Line 2.

Table 2
Modeled velocity and thickness in each layer of Line 1 and Line 2

| Layer | Line 1 | | Line 2 | |
|---|---|---|---|---|
| | Velocity (m/s) | Thickness (m) | Velocity (m/s) | Thickness (m) |
| 1 | 1000 | 1–32 | 1000 | 0–5 |
| 2 | 1675–1680 | 48–108 | 1610 | 103–112 |
| 3 | 1964–1987 | 64–125 | 2069–2071 | 103–105 |
| 4 | 2287–2289 | 188–263 | 2281–2282 | 97–108 |
| 5 | 2538–2540 | – | 2580 | – |

Fig. 4 shows the final velocity–depth models of Line 1 (N–S profile) and Line 2 (E–W profile) using the starting models in Fig. 3. The calculated velocities and thicknesses of the models are also illustrated in Table 2. The velocity–depth models for Line 1 and Line 2 are quite similar, consisting of a sequence of uniform layers, except for the differences in geometry. The velocity–depth models for both profiles are fairly homogeneous laterally, and velocity increases slowly with depth. The thick overburden at the north end of the final Line 1 model is consistent with the high topography along this portion of the profile. In contrast, the overburden is thin along the entire length of Line 2. Below the overburden (1000 m/s), a relatively sub-horizontal layer with average velocities of 1610–1680 m/s, ranging in thickness from 50 m to 112 m, is present on both profiles. The third layer in the structural sequence has a velocity of 1975–2070 m/s and is 65–125 m thick. The bottom of this layer dips to the north on Line 1, while it is quite flat on Line 2. Below layer 3, a layer with a wide thickness range (velocity of 2280–2290 m/s and 97–263 m thick) is present. On Line 1 it is structurally thicker than on Line 2. The geometry of this layer is less certain than the overlying layers. Below this variable velocity layer, a high-velocity layer (2540–2580 m/s) is present that the rays do not penetrate through with the given acquisition geometry. The velocity variation within the layers is probably due to lateral velocity variations since the resulting velocity within each layer is obtained from the control points along the profiles. The small range of velocity variation within each layer (<100 m/s) in both profiles indicates the small varying lateral velocity in this area.

Table 3
RMS traveltime residual of initial and final model of Line 1 and Line 2

| RMS traveltime residual (ms) | Line 1 | Line 2 |
|---|---|---|
| Initial model | 21.23 | 19.01 |
| Before short-wavelength static calculation | 12.66 | 4.03 |
| After short-wavelength static calculation | 7.03 | 3.75 |

The criteria used for estimating the accuracy of the reconstructed models in this study are the RMS values of traveltime residuals and a qualitative estimation of the ray density. For each iteration, data errors can propagate to the next iteration. RMS errors indicate how well the observed traveltime data are predicted by the obtained velocity models. In order to obtain more reliable models, residuals greater than two times the RMS error were deleted automatically after the first iteration, corresponding to about 3% of the picks. The inverse solutions fit the data reasonably well after 5 iterations, as seen on the time residuals graph in Fig. 5. Table 3 shows the RMS error continuously decreasing with increased iteration performed until convergence is reached and the short-wavelength static is calculated. It is interesting to note that the low signal-to-noise ratio of data and higher topography on Line 1 is probably the reason for the higher RMS error of Line 1 relative to Line 2. However, after the short-wavelength static calculation, the RMS error rapidly decreases, strongly indicating that short-wavelength refractions static corrections are important for seismic reflection processing of the line.

Brzostowski and McMechan (1992) and Stefani (1995) provide a qualitative estimation of model reliability. They found that the main distortions and ambiguities in the solution occur near the edges of the tomogram where ray coverage is generally extremely poor or absent. Therefore, these portions of the models have not been

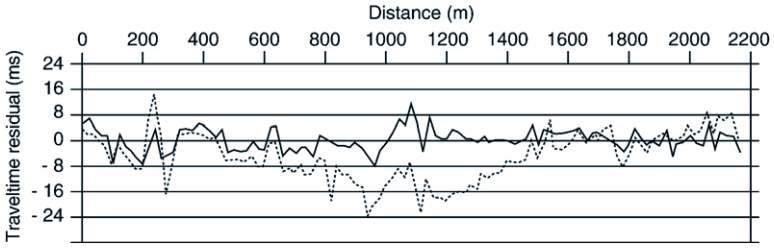


Fig. 5. Traveltime residuals of initial (dot line) and final models (solid line) for the shot shown in Fig. 2.

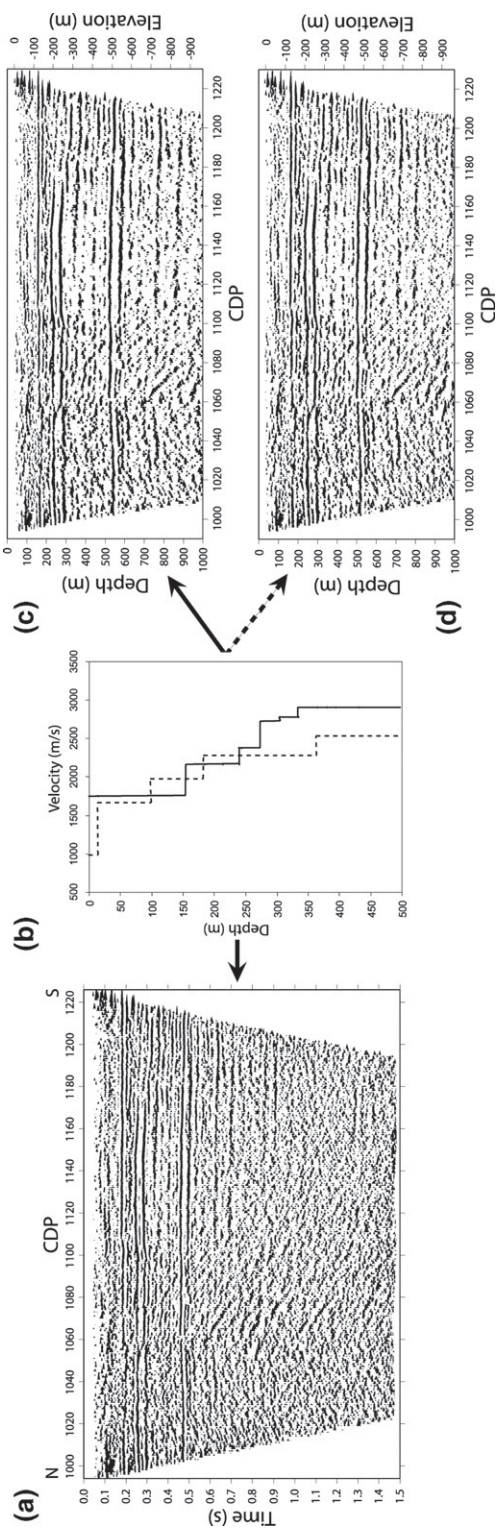


Fig. 6. (a) CDP stacked sections of Line 1. (b) Velocity function used for time to depth conversion of Line 1. Solid line is the Dix velocity function and the dashed line is the GLI velocity function. (c) Depth section converted by the Dix velocity function, and (d) depth section converted by the GLI velocity function.

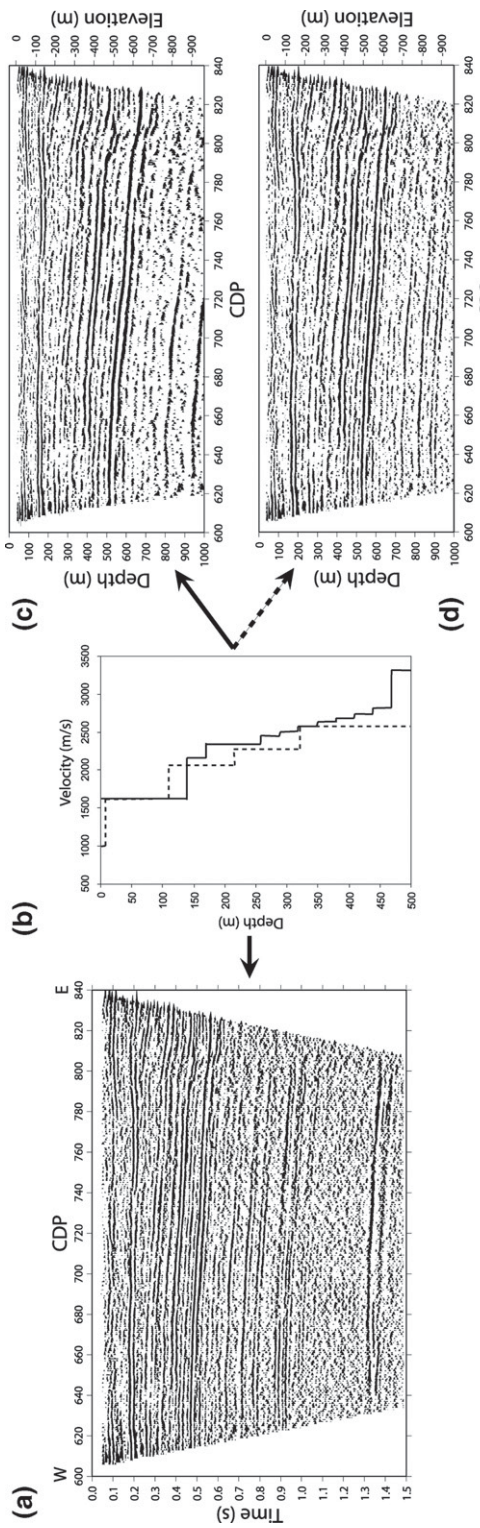


Fig. 7. (a) CDP stacked sections of Line 2. (b) Velocity function used for time to depth conversion of Line 2. Solid line is the Dix velocity function and the dashed line is the GLI velocity function. (c) Depth section converted by the Dix velocity function, and (d) depth section converted by the GLI velocity function.

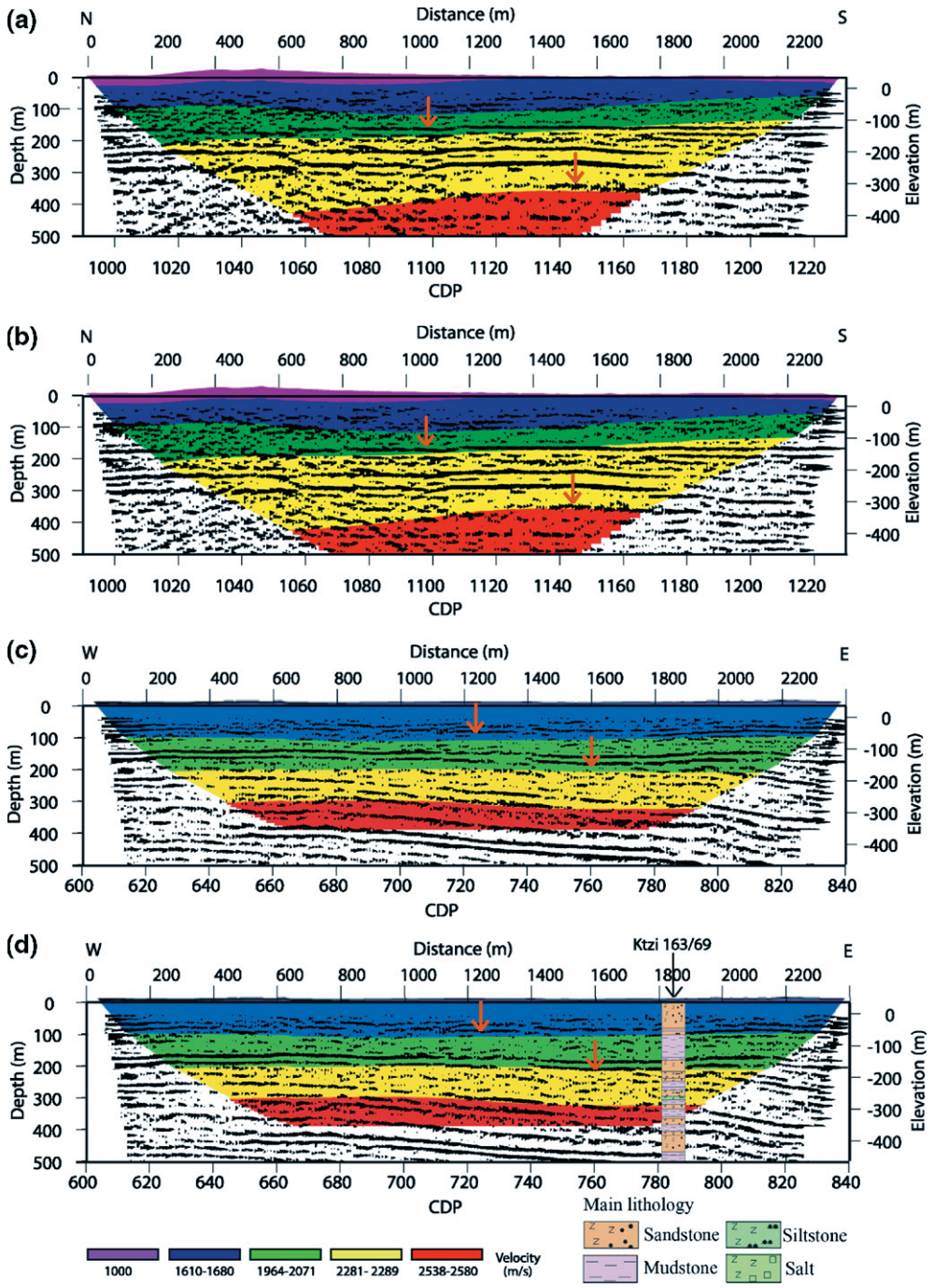


Fig. 8. Depth section overlain by the GLI model of Line 1 by using, (a) the Dix velocity and (b) the GLI velocity. Depth section overlain by GLI model of Line 2 by using (c) the Dix velocity and (d) the GLI velocity. Orange arrows mark examples of locations where the correlation between the depth section and the GLI model is better than with the Dix velocities. Geologic interpretation is constrained by information from the Ktzi 169/63 borehole.

displayed, nor considered in our interpretations. In a more quantitative manner, Zhu and Ebel (1994) estimated that the velocity distribution may be considered reliable for depths of 1/4 of the maximum source–receiver offset, or alternatively for depths from 1/2 up to 2/3 of the deepest ray penetration. By this estimation, our models are reliable down to depths of approximately 400 m. Moreover, we found that the mis-picks in our

data are often on the far offset traces, suggesting that the deeper parts of the models are the least reliable.

## 6. Discussion

We focus our discussion on the shallow portions of the reflection seismic sections, corresponding to depths from the surface down to about 400 m. In addition to the reflection seismic sections, we consider the velocity–depth models that we have obtained and geological data from a deep borehole in the area. The shallow sub-surface of the study area consists of sedimentary units that have distinct velocities, but with the velocity gradually increasing with depth within the units. Comparison of our velocity–depth models with CDP stacked sections shows consistent features in the shallow sub-surface between the two data sets. However, the shallowest portions of the reflection seismic images do not show the uppermost sedimentary units (Figs. 6a and 7a), due to the acquisition geometry used and partly to that the dominant frequency (30–100 Hz) of the seismic data is too low for imaging the uppermost 100 m. Figs. 6c and d and 7c and d show depth converted sections (unmigrated) obtained for Line 1 and Line 2 using (1) the stacking velocity from the CDP processing (solid line in Figs. 6b and 7b) and (2) the velocity–depth models obtained in this study (dashed line in Figs. 6b and 7b). Note that the images are similar, but that the layer thickness of the reflection seismic sections differs depending upon which velocity–depth model is used. The depths to the reflections obtained using the GLI velocity model are different than the depths obtained using the stacking velocity, implying a discrepancy between the two velocity functions. The Dix interval velocity of the upper 500 m and the GLI velocity–depth model of Line 1 and Line 2 are compared in Figs. 6b and 7b, respectively. In the upper 300 m there are only small differences in the interval velocities, but the layer boundaries of the GLI velocity model are somewhat shallower than the Dix velocity model from the CDP processing. Moreover, in the upper 150 m, only one layer is present in the Dix velocity model, while two layers are observed in the GLI velocity–depth model. Below 300 m, velocities in the Dix velocity are higher than in the GLI model. As mentioned earlier, layer velocities and geometries are less accurate for the deeper layers in the GLI model. Therefore, the Dix model may be more reliable below 300 m. In order to compare the GLI models directly with the reflection seismic sections they have been superimposed on top of the depth sections shown in Figs. 6 and 7 (Fig. 8). It is obvious that layer boundaries as defined by clear reflections on the seismic sections are more consistent with velocity boundaries from the GLI models obtained when using the velocity–depth models from this study compared to using the Dix velocities for depth conversion. This result indicates that the use of the GLI velocity fields produces a better time-to-depth conversion of the reflection data, at least in the upper 300 m. It should be noted that some reflectors have not been detected in our models (reflectors within the yellow zone in Fig. 8a and b). This is probably due to two reasons, (1) there is a possible fault zone between position 600–1200 m in Line 1, where the rays pass through a complex structure and (2) GLI is solved by a ray based approach, implying that the ray path is biased to high-velocity layers whereas the reflections may be due to low velocity zones. Correlation is better between layer boundaries where the reflector is clear (arrow marked at about 350 m depth in Fig. 8b). Another use for the GLI velocity models is as input for near-surface data processing since stacking velocities are commonly difficult to estimate in the near-surface due to reflection hyperbolas only being observed on a few traces (Miller et al., 1998).

Thick near-surface low velocity layers are problematic, both when inverting for the velocity–depth model and when processing the reflection seismic data, particularly Line 1. The poorer model restoration obtained on Line 1 is probably due to statics problems associated with the topographic high containing low velocity material. The significant decrease in the RMS error on Line 1 after inclusion of the short-wavelength static calculation is evidence for this. This suggests that solely using refraction based static corrections is not adequate and that improvement in the section can be obtained using a surface-consistent static method for handling short-wavelength variations (residual statics) in the reflection seismic processing. Bergman et al. (2004) demonstrated that where strong velocity contrasts exist in the near-surface the velocity model obtained from simultaneous inversion for static corrections and velocity structure produces the best estimate of the velocity model. In this study, the relatively strong velocity contrast between the low velocity overburden (1000 m/s) and the underlying layer (1600–1700 m/s) along with the near-surface static shifts may also be influencing the final velocity model. The latter is evidenced by the stacked sections being significantly improved by accounting for these near-surface static shifts (Yordkayhun et al., submitted for publication).

Geological interpretation based on the combination of our models, the reflection seismic sections and data from the Ktzi 163/69 deep borehole show that the upper

400 m of the sub-surface are represented by four groups of sediments. In general, the uppermost layer consists of low velocity (1000 m/s) unconsolidated sediment with a thickness varying from 5 m where topography is fairly flat to 15–30 m where topographic relief is high. Quaternary sandstone deposits with velocities of 1600–1700 m/s and 50–110 m thick are present below these unconsolidated sediments. The velocities suggest saturated soil material in a shallow aquifer as the composition of this layer. This unit is underlain by Tertiary deposits of mudstone with velocities of about 1950–2050 m/s and thickness ranging from 60 to 120 m. Below the Tertiary unit, Jurassic sedimentary sequences are represented by an alternating sequence of sandstone, mudstone and siltstone extending to depths of about 250–400 m and with velocities in the range of 2300–2600 m/s.

## 7. Conclusions

We have shown that the shallow velocity–depth models obtained from generalized linear inversion (GLI) of first arrival traveltime data reveal near-surface structure at the $CO_2$SINK site, Ketzin. The major advantage of this method is that the technique is simple, flexible and easy to handle. Geological structures defined by velocities and thicknesses can easily be modified. The velocity–depth models obtained provide additional constraints on the structure of the shallow sub-surface. In particular, a more detailed picture of the uppermost 200 m is obtained, that portion of the reflection seismic sections that suffer from poor coverage due to the acquisition geometry, source generated noise, and, possibly, the resolution of the data. The velocity–depth models may also be used to convert the reflection seismic sections from time to depth. Compared to using stacking velocities, the GLI velocity model based depth sections give a more consistent image of the sub-surface.

In addition to providing velocity–depth models, the GLI method allows for the calculation of short and long-wavelength statics. The benefit of this static information is that it can be used to improve the reflection seismic processing and aid in producing a more reliable time-to-depth conversion at early traveltimes.

Comparison of the reflection seismic data and the velocity models with borehole geology allows a reliable interpretation of the seismic data to be made. The sedimentary units are characterized by a gradual increase in velocity with depth with lateral velocity variations being insignificant, indicating a homogeneous near-surface.

Although the GLI models obtained in this study appear reliable, there are some limitations in the method. Firstly, thin layers or low velocity layers (hidden layers) cannot be determined from the traveltime observations. Secondly, because of the inherent non-uniqueness of traveltime inversion, the GLI method is dependent on the quality of the picked first arrivals, choice of initial model and the degree of near-surface lateral velocity variations. Finally, in order to be confident of the final solution, adequate a priori information is required for each particular case studied.

## Acknowledgements

We gratefully acknowledge the $CO_2$SINK project for providing access to supplementary data sets. We thank Hampson and Russell for supplying the GLI3D software. The European Commission is gratefully acknowledged for their funding of the "$CO_2$SINK — $CO_2$ Storage by Injection into a Natural Storage at Ketzin", Project No. 502599.

## References

Arts, R., Eiken, O., Chadwick, A., Zweigel, P., van der Meer, L., Zinszner, B., 2004. Monitoring of $CO_2$ injected at Sleipner using time-lapse seismic data. Energy 29, 1383–1392.

Bais, G., Bruno, P.G., Di Fiore, V., Rapolla, A., 2003. Characterization of shallow volcanoclastic deposits by turning ray seismic tomography: an application to the Naples urban area. Journal of Applied Geophysics 52, 11–21.

Belfer, I., Landa, E., 1996. Shallow velocity–depth model imaging by refraction tomography. Geophysical Prospecting 44, 859–870.

Bergman, B., Tryggvason, A., Juhlin, C., 2004. High resolution seismic traveltime tomography incorporating static corrections applied to a till-covered bed rock environment. Geophysics 69, 1082–1090.

Boschetti, F., Dentithz, M.C., List, R.D., 1996. Inversion of seismic refraction data using genetic algorithms. Geophysics 61, 1715–1727.

Brzostowski, M.A., McMechan, G.A., 1992. 3-D tomographic imaging of near-surface seismic velocity and attenuation. Geophysics 57, 396–403.

Buker, F., Green, A.G., Horstmeyer, H., 1998. Shallow seismic reflection study of a glaciated valley. Geophysics 63, 1395–1407.

Cosma, C., Enescu, N., 2001. Characterization of fractured rock in the vicinity of tunnels by the swept impact seismic technique. International Journal of Rock Mechanics and Mining Sciences 38, 815–821.

Förster, A., Norden, B., Zinck-Jørgensen, K., Frykman, P., Kulenkampff, J., Spangenberg, E., Erzinger, J., Zimmer, M., Kopp, J., Borm, G., Juhlin, C., Cosma, C., Hurter, S., 2006. Baseline characterization of the $CO_2$SINK geological storage site at Ketzin, Germany. Environmental Geosciences 13, 145–161.

Hampson, D., Russell, B., 1984. First-break interpretation using generalized linear inversion. Journal of the Canadian Society of Exploration Geophysicists 20, 40–54.

Hampson-Russell Software Services Ltd., 2004. GLI3D theory, 131 pp.

Juhlin, C., Giese, R., Zinck-Jørgensen, K., Cosma, C., Kazemeini, H., Juhojuntti, N., Luth, S., Norden, B., Förster, A., 2007. 3D baseline seismics at Ketzin, Germany: The $CO_2$SINK project. Geophysics 72, no. 5.

Juhlin, C., Palm, H., Mullern, C., Wallberg, B., 2002. Imaging of groundwater resources in glacial deposits using high-resolution reflection seismics, Sweden. Journal of Applied Geophysics 51, 107–120.

Lanz, E., Maurer, H., Green, A.G., 1998. Refraction tomography over a buried waste disposal site. Geophysics 63, 1414–1433.

Lines, L.R., Treitel, S., 1984. A review of least-squares inversion and its application to geophysical problems. Geophysical Prospecting 32, 159–186.

Macrides, C.G., Dennis, L.P., 1994. 2D and 3D refraction statics via tomographic inversion with under-relaxation. First Break 12, 523–537.

Marsden, D., 1993. Statics corrections—a review, part II. The Leading Edge 12 (2), 115–120.

Marti, D., Carbonell, R., Tryggvason, A., Escuder, J., Perez-Estaun, A., 2002. Mapping brittle fracture zones in three dimensions: high-resolution traveltime seismic tomography in a granitic pluton. Geophysical Journal International 149, 95–105.

Menke, W., 1984. Geophysical Data Analysis: Discrete Inverse Theory, Revised Ed. New York, Academic Press Inc. 289 pp.

IPCC, 2005. In: Metz, B., Davidson, O., de Coninck, H.C., Loos, M., Meyer, L. (Eds.), IPCC Special Report on Carbon Dioxide Capture and Storage. Prepared by Working Group III of the Intergovernmental Panel on Climate Change. Cambridge, UK, Cambridge University Press. 442 pp.

Miller, K.C., Harder, S.H., Adams, D.C., O'Donnel Jr., T., 1998. Integrating high-resolution refraction data into near-surface seismic reflection data processing and interpretation. Geophysics 63, 1339–1347.

Olsen, K.B., 1989. A stable and flexible procedure for the inverse modeling of seismic first arrivals. Geophysical Prospecting 37, 455–465.

Park, C.B., Miller, R.D., Steeples, D.W., Black, R.A., 1996. Swept impact seismic technique (SIST). Geophysics 61, 1789–1803.

Stefani, J.P., 1995. Turning-ray tomography. Geophysics 60, 1917–1929.

Scales, J.A., 1987. Tomographic inversion via the conjugate gradient method. Geophysics 52, 179–185.

Steeples, D.W., Miller, R.D., 1990. Seismic reflection methods applied to engineering, environmental, and groundwater problems. In: Ward, S.H. (Ed.), Geotechnical and Environmental Geophysics, I: Review and Tutorial. Soc. Expl. Geophys. pp. 1–30.

Taner, M.T., Wagner, D.E., Baysal, E., Lu, L., 1998. A unified method for 2-D and 3-D refraction statics. Geophysics 63, 260–274.

White, D.J., Burrowes, G., David, T., Hajnal, Z., Hirsche, K., Hutcheon, I., Majer, E., Rostron, B., Whittaker, S., 2004. Greenhouse gas sequestration in abandoned oil reservoirs: the International Energy Agency Weyburn pilot project. GSA Today 14, 4–10.

Yordkayhun, S., Ivanova, A., Giese, R., Juhlin, C., Cosma, C., submitted for publication. Comparison of surface seismic sources at the $CO_2$SINK site, Ketzin, Germany. Geophysical Prospecting.

Zhu, H., Ebel, J.E., 1994. Tomographic inversion for the seismic velocity structure beneath northern New England using seismic refraction data. Journal of Geophysical Research 99, 331–357.